Journal of Power Sources 262 (2014) 62–71

Contents lists available at ScienceDirect

Journal of Power Sources

journal homepage: www.elsevier.com/locate/jpowsour

Improved lithium-ion battery performance of $LiNi_{0.5}Mn_{1.5-x}Ti_xO_4$ high voltage spinel in full-cells paired with graphite and $Li_4Ti_5O_{12}$ negative electrodes

Jung-Hyun Kim [a,*], Nicholas P.W. Pieczonka [b], Yang-Kook Sun [c], Bob R. Powell [a]

[a] Chemical & Materials Systems Laboratory, General Motors Global R&D Center, Warren, MI 48090, USA
[b] Optimal CAE Inc, Plymouth, MI 48170, USA
[c] Department of Energy Engineering, Hanyang University, Seoul 133-791, South Korea

HIGHLIGHTS

- Effect of Ti-substitution on the electrochemical properties of $LiNi_{0.5}Mn_{1.5-x}Ti_xO_4$.
- $LiNi_{0.5}Mn_{1.5-x}Ti_xO_4$ showed improved cycle life in full-cells (vs. graphite or LTO).
- The Ti-substitution reduces electrolyte oxidation during battery cell operation.
- The Ti-substitution retards parasitic reactions at electrode/electrolyte interface.
- Among various samples, LNMT3 delivered optimal battery performances.

ARTICLE INFO

Article history:
Received 20 January 2014
Received in revised form
20 March 2014
Accepted 22 March 2014
Available online 29 March 2014

Keywords:
Ti substitution
High voltage (5 V) spinel
Full cells
Graphite
$Li_4Ti_5O_{12}$
Li-ion batteries

ABSTRACT

The effect of Ti-substitution on the electrochemical properties of $LiNi_{0.5}Mn_{1.5-x}Ti_xO_4$ was investigated by using half-cells paired with lithium metal, and full-cells paired with either graphite or $Li_4Ti_5O_{12}$ (LTO) negative electrodes. In half-cells, Ti-substitution increased the operation voltage, but reduced the specific capacity. While some improvements in performance, such as higher operation voltage and less self-discharge, could be measured in the half-cells, the critical advantages of the Ti-substitution were readily observed in full-cell cycling. Compared with Ti-free $LiNi_{0.5}Mn_{1.5}O_4$, the $LiNi_{0.5}Mn_{1.5-x}Ti_xO_4$ electrodes delivered improved full-cell performance whether paired with graphite or LTO negative electrodes; greater cycle life, higher cell operating voltage, and lower voltage polarization on charging/discharging. Based on relatively low self-discharge and high Coulombic efficiency, it is suggested that the Ti-substitution in $LiNi_{0.5}Mn_{1.5-x}Ti_xO_4$ retards electrolyte oxidation. In addition, scanning electron microscopy (SEM) images revealed that cycle-aged $LiNi_{0.5}Mn_{1.2}Ti_{0.3}O_4$ particle surfaces remained relatively clean compared with those of $LiNi_{0.5}Mn_{1.5}O_4$ particles. These results are consistent with the hypothesis that Ti-substitution reduces electrolyte oxidation and retards or prevents some of the degradative parasitic reactions at the electrode/electrolyte interfaces during battery cell operation.

1. Introduction

High voltage $LiNi_{0.5}Mn_{1.5}O_4$ (LNMO) spinel is a promising candidate as the positive electrode in next generation Li-ion batteries for electric vehicle applications due to its high operating voltage of ~4.7 V (vs. Li/Li^+) and good high-rate performance [1–3]. Unfortunately, the benefit of high voltage operation is difficult to realize because of oxidative decomposition of the electrolyte. Traditional positive electrode materials such as $LiCoO_2$ do not suffer from an oxidative decomposition of electrolytes because they operate at lower voltages; <4.5 V vs. Li [4]. Although LNMO/Li half cells deliver good battery performance, [1,2] recent studies have reported poor cycle life of LNMO/graphite full-cells, especially at elevated temperatures; higher than 45 °C [5–7]. The degradation of the full-cell performance is attributed to thermal and electrochemical decomposition of conventional electrolytes, which are typically blends of fluorinated lithium salts with carbonate-based solvents. It has been reported that the capacity fading is caused

* Corresponding author.
E-mail address: junghyun.kim@gm.com (J.-H. Kim).

http://dx.doi.org/10.1016/j.jpowsour.2014.03.107
0378-7753/

by the loss of active Li^+ due to parasitic reactions in full-cells [6,7]. Although detailed mechanisms are not fully understood, it has been suggested that several different products of electrolyte decomposition, such as HF, CO_2, and transition metal dissolution, contribute to the Li^+ loss [6,8,9].

Recent studies have reported that Ti doping can improve the battery performance of $LiNi_{0.5}Mn_{1.5-x}Ti_xO_4$ [10,11]. The substitution of Ti for Mn in $LiNi_{0.5}Mn_{1.5-x}Ti_xO_4$ suppresses Ni/Mn ordering, which increases the Li^+ ion diffusion rate [10]. Noguchi et al. [11] demonstrated that small amounts of Ti substitution ($x < 0.2$) for Mn improved the cycle lives of $LiNi_{0.5}Mn_{1.5-x}Ti_xO_4$/graphite full-cells. They showed that the capacity retention of the full-cells increased with Ti content in the range from $x = 0$ to 0.19. However, greater Ti substitution ($x \geq 0.5$) reduced the capacity and cycle life of $LiNi_{0.5}Mn_{1.5-x}Ti_xO_4$/Li half-cells, an effect which was attributed to a perturbation of the electron hopping pathway by the presence of Ti^{4+} (d^0) in the lattice [10]. Fig. 1 shows the variation of discharge capacity with Ti content in $LiNi_{0.5}Mn_{1.5-x}Ti_xO_4$/Li half-cells. However, the capacity retentions of $LiNi_{0.5}Mn_{1.5-x}Ti_xO_4$/graphite full-cells are unknown yet for Ti contents higher than 0.2, and below 0.5. In this study, we investigated the full-cell performance of the $LiNi_{0.5}Mn_{1.5-x}Ti_xO_4$ for $x = 0.3$, 0.35, and 0.4 paired with graphite and $Li[Li_{1/3}Ti_{5/3}]O_4$ (LTO) negative electrodes.

2. Experimental

$LiNi_{0.5}Mn_{1.5-x}Ti_xO_4$ was synthesized via solid-state reaction. Stoichiometric amounts of Li_2CO_3, $NiCO_3$, $MnCO_3$, and TiO_2 were mixed using a ball-mill (SPEX 8000D) for 30 min. The mixed precursors were pelletized and heated at 500 °C for 12 h in air. The resulting powders were reground, pelletized, and heated at 650 °C for 12 h in air. This synthesis was completed with a final heat treatment at 900 °C for 6 h in air. The 900 °C treatment yields LNMO and $LiNi_{0.5}Mn_{1.5-x}Ti_xO_4$ with fully disordered Ni/Mn, but it can also yield various rock salt-phase impurities. Annealing at 700 °C for 48 h removes these impurity phases. Accordingly, Ti-substituted samples ($x = 0.3$, 0.35, and 0.4) were annealed at 700 °C for 48 h. The Ti-free ($x = 0$) samples were not annealed at 700 °C to prevent Ni/Mn ordering, which has been observed and which reduces electrochemical performance compared with fully disordered Ni/Mn in LNMO [1,10]. Earlier study showed that Ti substitution in LNMO helped retain Ni/Mn disorder, as evidenced by XRD and TEM analyses [10]. Surface areas of as-prepared LNMO and $x = 0.3$, respectively, were determined to be 1.112 and 1.154 $m^2\ g^{-1}$ by Brunauer–Emmett–Teller (BET) analysis. Table 1 lists the nomenclatures of the various samples investigated in this report. Fourier transform infrared (FT-IR) spectra were acquired with a Nicolet instrument with 2 cm^{-1} resolution using KBr pellets containing 0.5 wt% $LiNi_{0.5}Mn_{1.5-x}Ti_xO_4$ powders.

The positive electrode consisted of 80:10:10 wt% of $LiNi_{0.5}Mn_{1.5-x}Ti_xO_4$, super-P carbon, and polyvinylidene fluoride (PVDF, Kynar HSV900). For half-cells, lithium foil was used as the anode. For $LiNi_{0.5}Mn_{1.5-x}Ti_xO_4$/graphite full-cells, the graphite negative electrode consisted of 89:4:7 wt% of graphite (G8, Conocophillips), super-P carbon, and PVDF. For $LiNi_{0.5}Mn_{1.5-x}Ti_xO_4$/LTO full-cells, the $Li_4Ti_5O_{12}$ (LTO) negative electrode consisted of 80:10:10 wt% of LTO, super-P carbon, and PVDF. Each electrode formulation was mixed with N-methylpyrrolidone (NMP) and coated onto Al (for LNMO) or Cu (for graphite and LTO) foil via the doctor-blade method. A piece of separator (Celgard, PP/PE/PP trilayer), and a 1 M $LiPF_6$ in ethylene carbonate (EC)/ethyl methyl carbonate (EMC) (1/1 vol. ratio) electrolyte were used for preparing coin cells. All coin cells were cycled using a Maccor 4000 battery testing system. Scanning electron microscopy (SEM, Zeiss NVision) images of cycle-aged $LiNi_{0.5}Mn_{1.5-x}Ti_xO_4$ ($x = 0$ and 0.3) electrodes were acquired.

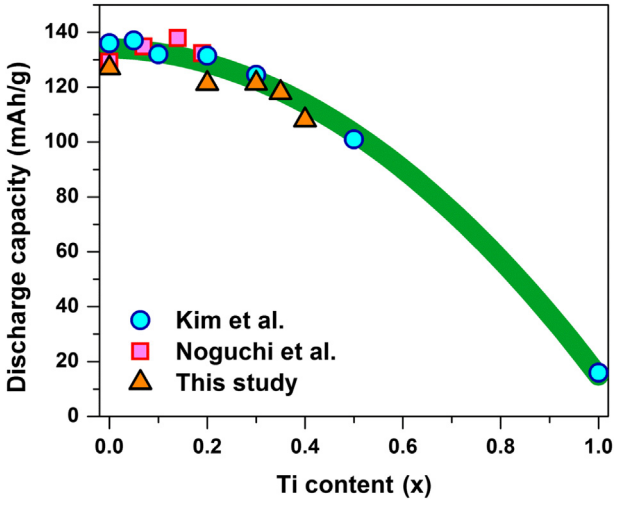

Fig. 1. The variation of discharge capacity with Ti content measured from $LiNi_{0.5}Mn_{1.5-x}Ti_xO_4$/Li half-cells. The data in this study were compared with the literature data from Kim et al. [10] and Noguchi et al. [11].

3. Results and discussion

3.1. Ni/Mn disordering in $LiNi_{0.5}Mn_{1.5-x}Ti_xO_4$

Fig. 2 shows the FT-IR spectra of the various $LiNi_{0.5}Mn_{1.5-x}Ti_xO_4$ samples. The Ni/Mn disordered LNMO spinel was synthesized using a final heat-treatment at 900 °C. To promote the Ni/Mn ordering, the LNMO powder was then annealed at 700 °C for 48 h [1,3,12,13]. The disordered LNMO prepared at 900 °C exhibited several broad and ill-defined bands mainly attributed to Mn–O and Ni–O bond vibrations. For the ordered LNMO, however, peaks at 555 cm^{-1} associated with the Mn–O vibration and 582–591 cm^{-1} associated with the Ni–O vibration are clearly defined [12]. The increase in the distinguishable peaks is the result of a reduction of space symmetry from disordered to ordered phase and subsequent increase in IR active bands [12]. Despite annealing at 700 °C for 48 h, the LNMT3 and LNMT35 samples exhibited spectra close to the disordered LNMO (900 °C). This can be explained by the reduction of Mn content by Ti substitution and subsequent perturbation of the 1/3 ratio of Ni/Mn required for ordering. The LNMT2 sample still exhibited noticeable peaks at 586 and 555 cm^{-1}, but their intensities are lower compared with the ordered LNMO (700 °C). This result suggests that the LNMT2 sample consists of both disordered and ordered spinel phases. The LNMT25 ($x = 0.25$) also showed the mixture of disordered and ordered spinels (data not shown here).

Table 1
List of samples and nomenclatures of various $LiNi_{0.5}Mn_{1.5-x}Ti_xO_4$ samples.

Nomenclatures	Sample descriptions
LNMO	$LiNi_{0.5}Mn_{1.5}O_4$ (LNMO) powder sample synthesized at 900 °C
LNMT2	$LiNi_{0.5}Mn_{1.3}Ti_{0.2}O_4$ synthesized at 900 °C followed by annealing at 700 °C for 48 h
LNMT3	$LiNi_{0.5}Mn_{1.2}Ti_{0.3}O_4$ synthesized at 900 °C followed by annealing at 700 °C for 48 h
LNMT35	$LiNi_{0.5}Mn_{1.15}Ti_{0.35}O_4$ synthesized at 900 °C followed by annealing at 700 °C for 48 h
LNMT4	$LiNi_{0.5}Mn_{1.1}Ti_{0.4}O_4$ synthesized at 900 °C followed by annealing at 700 °C for 48 h

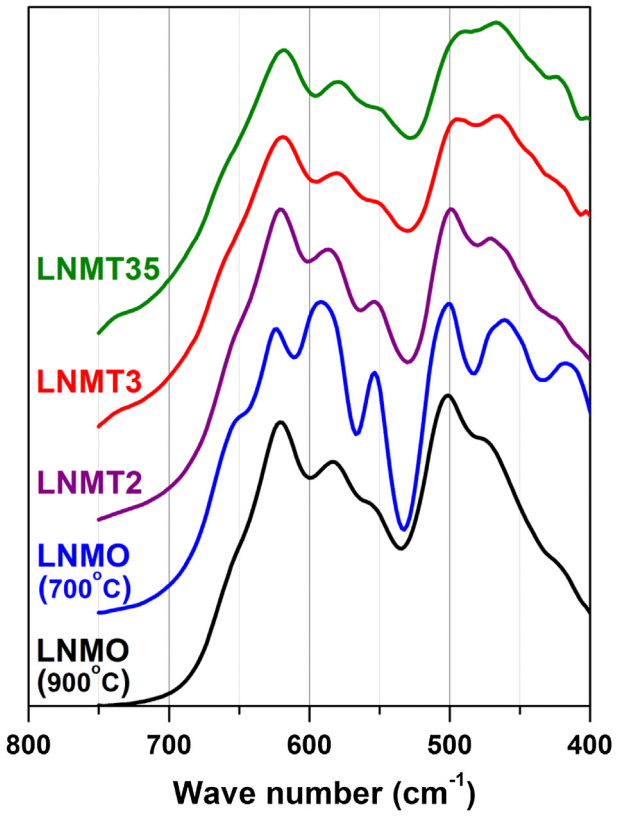

Fig. 2. Comparison of FT-IR spectra of LNMO and LNMTO samples. For the LNMO samples, two different final heat-treatments were applied: 900 °C for 6 h and 700 °C for 48 h. The LNMT2, LNMT3, and LNMT35 samples were heated at 700 °C for 48 h.

In conclusion, the $LiNi_{0.5}Mn_{1.5-x}Ti_xO_4$ sample is fully disordered for $x \geq 0.3$ with our experimental conditions. This result is slightly different than an earlier report, [10] as we found that starting precursors for the solid-state reaction synthesis can also affect the ordering behavior of $LiNi_{0.5}Mn_{1.5-x}Ti_xO_4$ spinels for $x < 0.3$.

3.2. $LiNi_{0.5}Mn_{1.5-x}Ti_xO_4$/Li half-cells

The effect of Ti substitution in $LiNi_{0.5}Mn_{1.5-x}Ti_xO_4$ on battery performance was assessed using coin-cells. Fig. 3(a) compares voltage profiles of $LiNi_{0.5}Mn_{1.5-x}Ti_xO_4$/Li half-cells on discharging. As shown in Fig. 1, the Ti-substituted $LiNi_{0.5}Mn_{1.5-x}Ti_xO_4$ ($x = 0.2$–0.4) electrodes delivered lower discharge capacity with increasing Ti content. As the result of annealing at 700 °C, the $LiNi_{0.5}Mn_{1.5-x}Ti_xO_4$ ($x = 0.2$–0.4) electrodes showed negligible capacity at ~4 V regions (associated with $Mn^{3+/4+}$ redox) compared with the Ti-free LNMO electrode. Meanwhile, the Ti substitution in $LiNi_{0.5}Mn_{1.5-x}Ti_xO_4$ increased the $Ni^{2+/4+}$ redox potentials, as evidenced by differential capacity profiles (dQ/dV) in Fig. 3(b). For example, the $Ni^{2+/3+}$ and $Ni^{3+/4+}$ redox voltages, respectively, increased from 4.686 V (for the LNMO) to 4.739 V (for the LNMT3) and from 4.753 V (for the LNMO) to 4.787 V (for the LNMT3) on charging. Unlike other samples, the LNMT2 electrode showed two separated peaks (at 4.725 V and 4.748 V on charging) which are associated with the $Ni^{2+/3+}$ redox. This peak splitting can be explained by individual contributions from disordered (4.725 V) and ordered (4.748 V) spinel phases for the $Ni^{2+/3+}$ redox, because the LNMT2 sample consisted of their mixed phases, as evidenced by the FT-IR data (see, Fig. 2). Since the potentials of the $Ni^{3+/4+}$ redox are similar between the disordered and ordered phases, [1] the

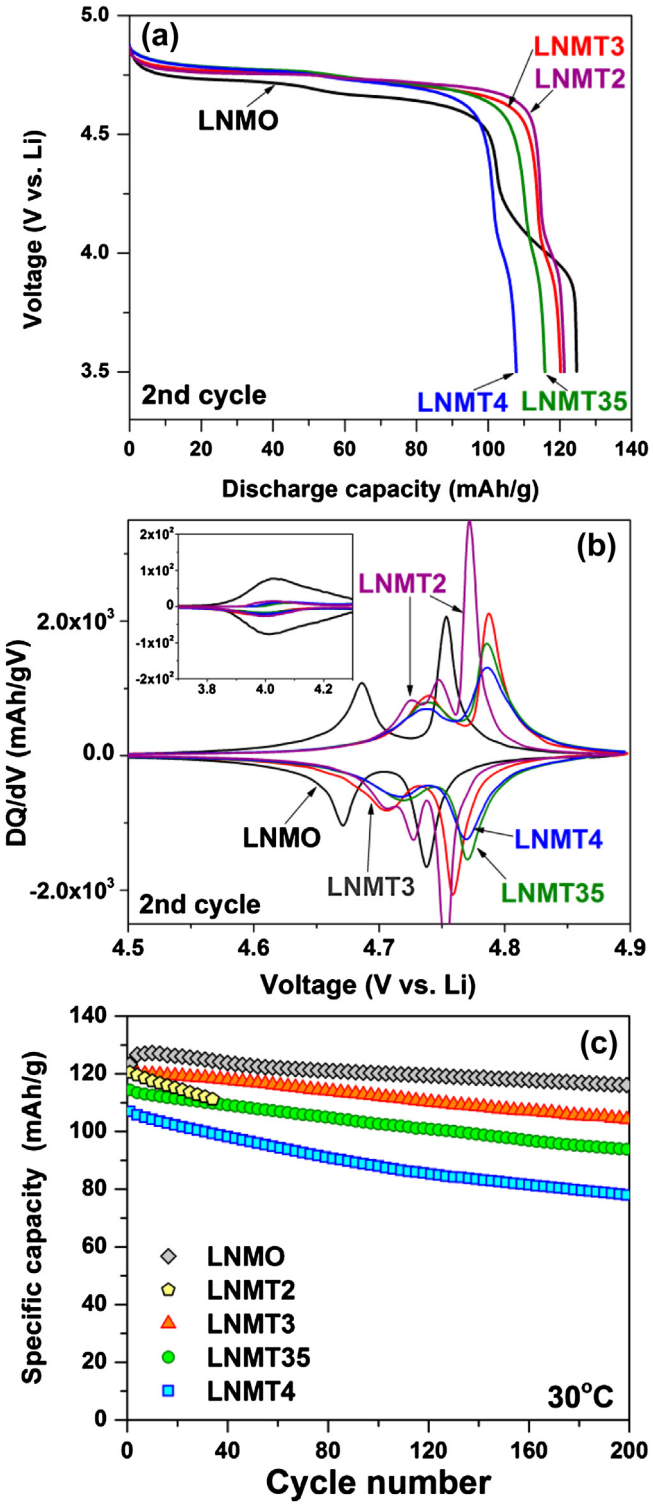

Fig. 3. (a) Comparison of voltage profiles measured from half-cells with C/10-rate at 30 °C and (b) their differential capacity profiles (dQ/dV). (c) Cycling performance of half-cells with C/5-rate at 30 °C.

LNMT2 electrode exhibited single redox peak at 4.772 V on charging.

Fig. 3(c) shows capacity retention of the $LiNi_{0.5}Mn_{1.5-x}Ti_xO_4$/Li half-cells during cycling with a C/5-rate at 30 °C. The LNMO delivered the highest discharge capacity of ~125 mAh g^{-1} and maintained ~92% of the initial capacity at the 200th cycles. The Ti

substitution in the $LiNi_{0.5}Mn_{1.5-x}Ti_xO_4$ lowered the initial capacities and capacity retentions. The LNMT3 and LNMT35 electrodes, respectively, showed initial discharge capacities of 121 mAh g^{-1} and 115 mAh g^{-1}, and exhibited 87% and 85% of capacity retentions at the 200th cycle. The LNMT4 electrode delivered an initial discharge capacity of 108 mAh g^{-1} and 72% of capacity retention at the 200th cycle. The LNMT2 electrode delivered poor capacity retention compared with other electrodes. This can be explained partly by the presence of the ordered phase, which has been shown to deteriorate the cycle life of battery cells [14]. In general, the decreases in capacity and cycle life of the $LiNi_{0.5}Mn_{1.5-x}Ti_xO_4$ electrode with Ti content agree well with that reported in the literature [10,15].

The high operation voltage of the $LiNi_{0.5}Mn_{1.5-x}Ti_xO_4$ spinel is a critical issue for conventional liquid electrolytes [4]. Electrolyte oxidation occurs through contact with partly or fully delithiated LNMO electrodes at high voltages (i.e. ~4.7 V), which results in a self-discharge of the LNMO electrode (Eq. (1)) as evidenced by electrochemical, XRD, and Raman spectroscopy data [7,16,17].

$$Ni_{0.5}Mn_{1.5}O_4 + x\,Li^+ + x\,\text{electrolyte} \rightarrow Li_xNi_{0.5}Mn_{1.5}O_4 + x\,\text{electrolyte}^+ \quad (1)$$

The effect of Ti substitution on the oxidative electrolyte decomposition and subsequent self-discharge was investigated by the following methods. The $LiNi_{0.5}Mn_{1.5-x}Ti_xO_4$/Li half-cells were fully charged to 4.9 V, and rested for 72 h in open circuit condition, as illustrated in Fig. 4(a). During the 72 h period, any electrolyte oxidation will donate electrons to the $Ni_{0.5}Mn_{1.5-x}Ti_xO_4$, which results in $Ni^{4+} \rightarrow Ni^{3+}$ reduction with Li^+ accommodation in the $Ni_{0.5}Mn_{1.5-x}Ti_xO_4$ (self-discharge). After the 72 h rest period, the half-cells were discharged to 3.5 V, and were found to deliver a lower discharge capacity (C_{SD}) than their usual (C_{Normal}) capacity due to the impact of self-discharge. Considering Eq. (1), it will be reasonable to assume that the self-discharge capacity, determined by subtracting C_{SD} from C_{Normal}, will be proportional to the degree of oxidative decomposition of electrolyte. Fig. 4(b) and (c) illustrates the self-discharge capacity from the *dQ/dV* profiles of LNMO and LNMT35 half-cells. The shaded area (highlighted in blue (in the web version)) corresponds to the amount of self-discharge, the difference between C_{SD} (red line, normal cycle (in the web version)) and C_{Normal} (black line, self-discharge cycle).

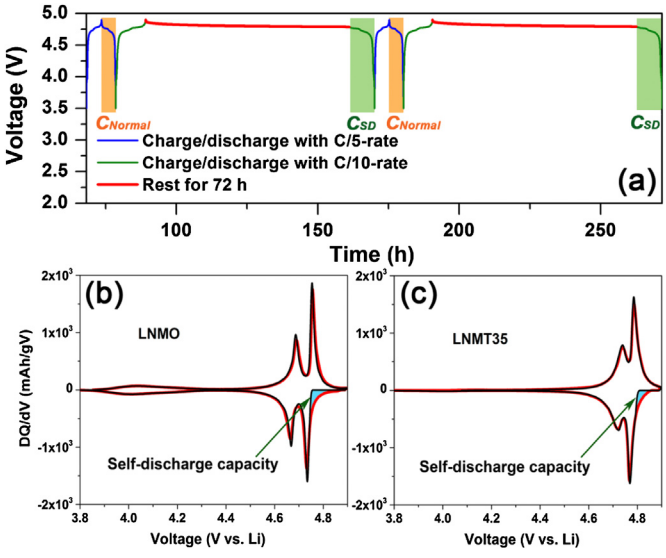

Fig. 4. (a) Representative voltage profiles of a half-cell with 72 h intervals at fully charged state (4.9 V vs. Li) to assess the self-discharge capacity ($C_{SD} - C_{Normal}$). Comparison of *dQ/dV* profiles with and without the 72 h intervals at fully-charged state for (b) LNMO/Li and (c) LNMT35/Li half-cells at 30 °C. Shaded region corresponds to the self-discharge capacity.

The aforementioned self-discharge tests were repeated 10 times for the $LiNi_{0.5}Mn_{1.5-x}Ti_xO_4$/Li half-cells at 30 °C. Fig. 5 shows the effect of Ti substitution on the self-discharge capacities during cycling. The LNMO electrode delivered the highest initial self-discharge capacity of 16 mAh g^{-1} among the electrodes tested, indicating the largest amount of electrolyte oxidation. With increasing Ti content, the initial self-discharge amount decreased for the $LiNi_{0.5}Mn_{1.5-x}Ti_xO_4$ electrodes from $x = 0$ to 0.35. This result suggests that the Ti-substituted $LiNi_{0.5}Mn_{1.5-x}Ti_xO_4$ electrodes oxidize the electrolyte less than the LNMO electrode does. It is noteworthy that all the cells exhibit a trend of decreasing self-discharge with increasing number of cycles. This result possibly suggests a formation of passivation layer on electrodes as a result of electrolyte decomposition. The effectiveness of such passivation layer and its stability upon repeated cycling need to be investigated in future studies.

The half-cell data suggest that the Ti-substitution for Mn in $LiNi_{0.5}Mn_{1.5-x}Ti_xO_4$ offers a trade-off between half-cell battery performances (specific capacity and cycle life) and electrolyte stability. However, half-cell data is inadequate to identify the main degradation source of the high-voltage spinel because any Li^+ loss in the cell is compensated by the lithium metal electrode. In this regard, the electrochemical properties of the $LiNi_{0.5}Mn_{1.5-x}Ti_xO_4$ samples were further investigated using full-cells, paired with either graphite or LTO negative electrodes.

3.3. $LiNi_{0.5}Mn_{1.5-x}Ti_xO_4$/graphite full-cells

The $LiNi_{0.5}Mn_{1.5-x}Ti_xO_4$/graphite full-cells were cycled in a voltage range of 3.4–4.8 V with C/5-rate at 30 °C. The resulting voltage profiles of the full-cells are shown in Fig. 6. Fig. 6(a) shows that the LNMT3 and LNMT4 electrodes delivered higher cell voltages compared with those of LNMO due to their higher $Ni^{2+/4+}$ redox voltages (see, Fig. 3). The LNMO electrode showed capacity at around 4 V at the 5th cycle, which gradually decreased with further cycling and disappeared after ~30 cycles. After ~30 cycles, the LNMO electrode started to lose its capacity from the 4.4–4.7 V regions. Our earlier reports revealed that the capacity fading is

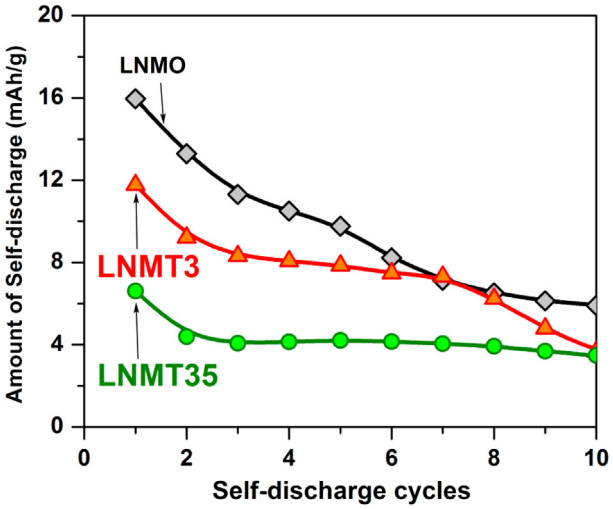

Fig. 5. Comparison of self-discharge capacities from $LiNi_{0.5}Mn_{1.5-x}Ti_xO_4$/Li half-cells.

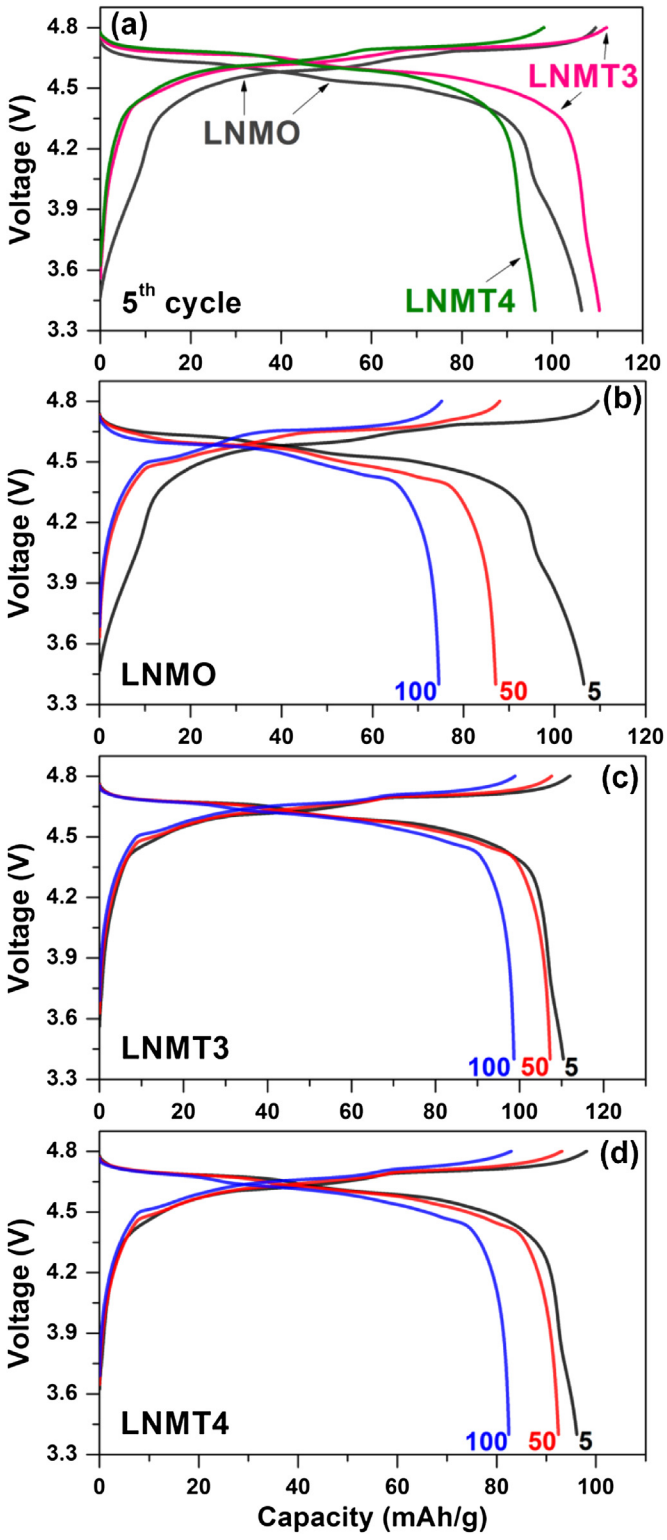

Fig. 6. (a) Representative voltage profiles of $LiNi_{0.5}Mn_{1.5-x}Ti_xO_4$ ($x = 0$, 0.3, and 0.4)/graphite full-cells at the 5th cycle at 30 °C. Variation of voltage profiles in the full-cells with (b) LNMO, (c) LNMT3, and (d) LNMT4 positive electrodes at 5th, 50th, and 100th cycles. All the full-cells were cycled in a voltage range of 3.4–4.8 V with C/5-rate at 30 °C.

caused by the loss of active Li^+ due to parasitic reactions in full-cells [6,7]. It has been reported that several different electrolyte decomposition products such as HF, CO_2, and transition metal dissolution may be responsible for the Li^+ loss [6,8,9].

Fig. 7(a) compares the capacity retentions of $LiNi_{0.5}Mn_{1.5-x}Ti_xO_4$/graphite full-cells at 30 °C. The LNMO sample exhibited rapid capacity fading with cycling. The Ti-substituted $LiNi_{0.5}Mn_{1.5-x}Ti_xO_4$ electrodes showed improved capacity retention and Coulombic efficiencies compared with those of the LNMO. For example, the LNMT3 and LNMT35 electrodes showed ca. 87–89% of capacity retention after 100 cycles, while the LNMO electrode showed 72% of capacity retention. The LNMT2 showed poor capacity retention due to the presence of ordered phase as discussed earlier. As shown in Fig. 7(b), the LNMT3 and LNMT35 electrodes exhibited ~99.7% Coulombic efficiencies (after stabilization), while the LNMO electrode exhibited ~99.1% in full-cells. In particular, the LNMT3, LNMT35, and LNMT4 electrodes retained much higher capacities compared with that of the LNMO electrode during the initial 50 cycles, as clearly shown in Fig. 6(b)–(d). However, the parasitic reactions in the full-cells and consequent Li^+ loss were inevitable during extended cycles, and resulted in the capacity losses beyond the 50th cycle. Earlier studies demonstrated that the capacity fading in Li-ion battery cells occurs due to various factors; e.g., unbalanced cathode/anode ratio, active material loss, self-discharge, overcharge, electrolyte side reactions [18–20]. In these factors, our recent study demonstrated that the electrolyte side reaction will be the main cause of the capacity fading in LNMO/graphite cells at 30 °C

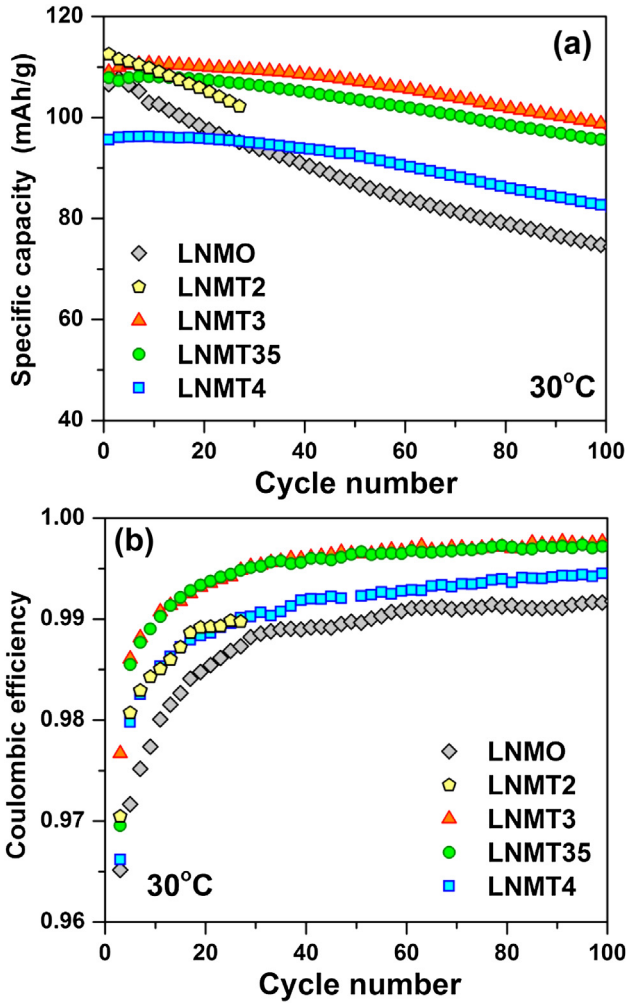

Fig. 7. (a) Cycling performances and (b) corresponding Coulombic efficiencies of $LiNi_{0.5}Mn_{1.5-x}Ti_xO_4$/graphite full-cells with C/5-rate at 30 °C.

[8]. The capacity fading mechanism in LNMO/graphite full-cells has been explained by following sequential reactions; (i) electrolyte oxidation at the LNMO surface, (ii) migration of the side-reaction products toward the graphite anode, and (iii) consumption of Li^+ via parasitic reactions at the electrolyte/graphite interface [21].

Fig. 8 shows the variations of mean voltages on charge/discharge with cycle number for the $LiNi_{0.5}Mn_{1.5-x}Ti_xO_4$/graphite full-cells. The LNMO full-cell showed increases in mean voltages on charge/discharge during initial ~30 cycles because of the aforementioned capacity loss at ~4 V regions; as the consequence of Li^+ loss, LNMO cannot be fully discharged at the end of discharge, which leads to the disappearance of the ~4 V plateau. The LNMO electrode showed a rapid increase in polarization between mean charge and discharge voltages ($V_{Gap/LNMO}$) until the 30th cycle, and maintained a relative large polarization compared with that measured for Ti-substituted samples. It is probable that parasitic reactions at the surfaces of LNMO and graphite SEI in the LNMO/graphite full-cell will be responsible for the increase in the polarization. In contrast, LNMT3, LNMT35, and LNMT4 electrodes maintained relatively small polarizations during cycling, which are attributed to less electrolyte oxidation and less parasitic reactions in the full-cells compared with the LNMO full-cell. In contrast, the LNMT2 delivered larger polarization compared with other Ti-substituted electrodes.

At an elevated temperature of 45 °C, the $LiNi_{0.5}Mn_{1.5-x}Ti_xO_4$/graphite full-cells deliver inferior battery performances compared with that obtained at 30 °C. This may be attributed to combined effects of electrochemical and thermal degradations in the electrolytes. For example, hydrolysis of $LiPF_6$ is promoted at elevated temperatures, which results in production of PF_5 and HF, sources of various parasitic reactions [22–27]. Fig. 9(b) shows capacity retentions of $LiNi_{0.5}Mn_{1.5-x}Ti_xO_4$/graphite full-cells measured during cycling with C/5-rate at 45 °C. The LNMT3 full-cell delivered the highest initial capacity of 115 mAh g^{-1}. The LNMO full-cell delivered a little lower initial capacity of 105 mAh g^{-1} followed by LNMT4 full-cell showing 100 mAh g^{-1}. The LNMO full-cell showed large capacity loss during the initial cycle compared with those of LNMT3 and LNMT4 at 45 °C, which will be related with parasitic reactions at electrode surfaces. Fig. 9 compares the battery performances of $LiNi_{0.5}Mn_{1.5-x}Ti_xO_4$/graphite full-cells at 45 °C. Fig. 9(c) shows that

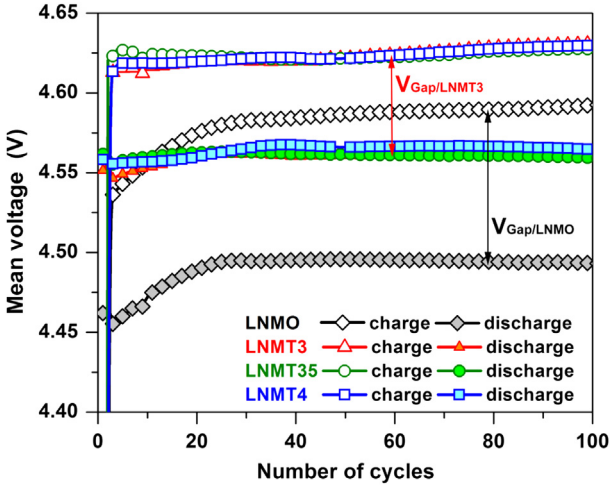

Fig. 8. Variations of mean voltages on charge (open) and discharge (closed) with number of cycles recorded from $LiNi_{0.5}Mn_{1.5-x}Ti_xO_4$/graphite full-cells with C/5-rate at 30 °C. Arrows are guide for eyes showing polarizations of mean voltages between charge and discharge.

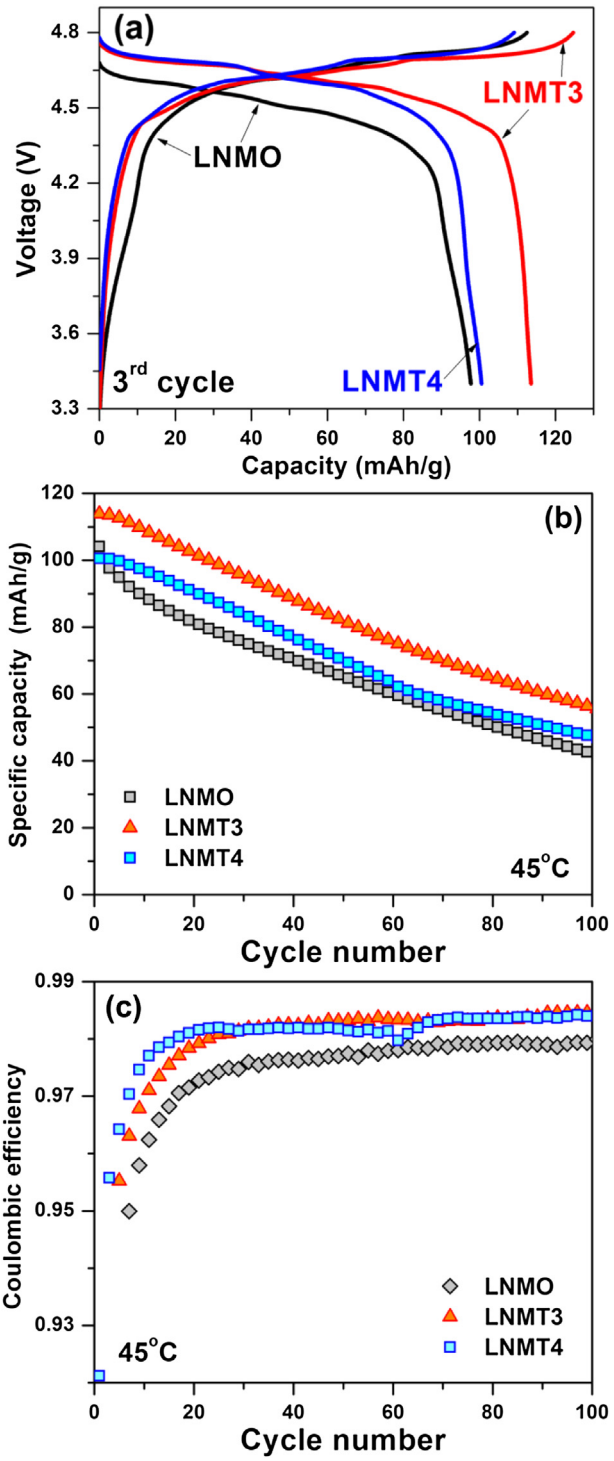

Fig. 9. (a) Representative voltage profiles of $LiNi_{0.5}Mn_{1.5-x}Ti_xO_4$ ($x = 0$, 0.3, and 0.4)/graphite full-cells at the 3rd cycle at 45 °C. (b) Cycling performances and (c) Coulombic efficiencies of the full-cells with C/5-rate at 45 °C.

the LNMT3 and LNMT4 electrodes exhibit higher Coulombic efficiencies (stabilized at 98.3%) than that of the LNMO (stabilized at 97.9%).

However, unlike the data obtained at 30 °C (see Fig. 7(a)), the slope of capacity retention at 45 °C was not improved by Ti substitution. The low Coulombic efficiencies indicate more severe electrolyte decomposition and parasitic reactions at 45 °C

compared with those at 30 °C. Therefore, any improvements in full-cells as a result of the Ti substitution will be obscured at 45 °C because severe electrolyte degradation is the dominant mechanism for capacity fading. For example, when EC/DEC (1/2 vol. ratio) was used, which has inferior thermal stability compared with the EC/EMC (1/1 vol. ratio) used in this study [27], all the full-cells failed within 20 cycles and cell data was not comparable with each other. However, it should be noted that the failure of LNMO/graphite full-cells is not only caused by thermal degradation but also oxidative decomposition of electrolytes; because the same EC/DEC (1/2 vol. ratio) based electrolyte delivered good capacity retentions in full-cells with lower operation voltages (i.e. $LiNi_{1/3}Co_{1/3}Mn_{1/3}O_2$/graphite) at 45 °C. Employing advanced electrolyte with improved thermal stability and wide applicable voltage window will be necessary to properly gauge the effect of Ti substitution on the $LiNi_{0.5}Mn_{1.5-x}Ti_xO_4$/graphite performances at elevated temperatures.

3.4. $LiNi_{0.5}Mn_{1.5-x}Ti_xO_4$/LTO full-cells

The $LiNi_{0.5}Mn_{1.5-x}Ti_xO_4$/graphite full-cell operation requires broad electrolyte stability windows ranging from 0 to 5 V vs. Li. The higher operation voltage of LTO negative electrode (ca. 1.5 V vs. Li) than that of the graphite (ca. 0.15 V vs. Li) can mitigate reductive decomposition of electrolyte, which would be beneficial for extending cycle life of $LiNi_{0.5}Mn_{1.5-x}Ti_xO_4$/LTO full-cell. Therefore, the effects of Ti substitution on the electrochemical properties of $LiNi_{0.5}Mn_{1.5-x}Ti_xO_4$/LTO full-cells were investigated at 30 and 45 °C.

Fig. 10(a) compares voltage profiles of the $LiNi_{0.5}Mn_{1.5-x}Ti_xO_4$/LTO full-cells at 30 °C. Again, LNMT3–LNMT4 electrodes exhibited higher cell voltage compared with the LNMO due to the higher $Ni^{2+/4+}$ redox voltages (see Fig. 3(b)). Fig. 10(b) shows the capacity retentions of $LiNi_{0.5}Mn_{1.5-x}Ti_xO_4$/LTO full-cells cycled with C/5-rate at 30 °C. The LNMO/LTO full-cell showed 93% capacity retention after 200 cycles, which is much higher than that of the LNMO/graphite full-cell (72% after 100 cycles). The LNMT3 and LNMT35 electrodes delivered high capacity retentions of ca. 96% and improved Coulombic efficiencies compared with those of the LNMO electrode. All the $LiNi_{0.5}Mn_{1.5-x}Ti_xO_4$/LTO full-cells finally reached similar Coulombic efficiency values in a range of 99.3–99.5% after 200 cycles. The low capacity retention of the LMNT4 full-cell cannot be explained at this time. It is possible that it is related to the reduced electronic conductivity, which was discussed in earlier with reference to Fig. 3(c).

Fig. 11 compares voltage profiles of the $LiNi_{0.5}Mn_{1.5-x}Ti_xO_4$/LTO full-cells at 45 °C. At the elevated temperature of 45 °C, the LNMO/LTO full-cell experienced significant capacity loss during cycling. Fig. 12(a) shows that the LNMO/LTO cell retains 58% capacity after 100 cycles at 45 °C. This noticeable capacity fading suggests that severe electrolyte decomposition problem still exists in the LNMO/LTO full-cell system at the elevated temperature. The variation in differential capacity profiles (dQ/dV) with cycle number in the LNMO/LTO full-cell is illustrated in Fig. 13. The LNMO/LTO full-cell first lost its capacity gradually at ~2.5 V regions ($Mn^{3+/4+}$ redox) during initial 40 cycles (see Fig. 13(a)), followed by a loss of capacity at the ~3.2 V regions ($Ni^{2+/4+}$ redox) onward (see Fig. 13(b)). This trend is the same as that observed from the LNMO/graphite full-cell [6], inferring that the capacity loss will be attributed to the loss of active Li^+ in the LNMO/LTO full-cell. Recent study by Belharouak et al. [28] showed a performance degradation of $LiMn_2O_4$/LTO full-cells at elevated temperatures. In addition to gaseous products (i.e. H_2, CO_2, etc.), they found Li_2TiF_6, manganese, fluorine, and phosphorous species on the surface of LTO, of which formation was promoted at high temperature and voltage [28]. Considering higher voltage of LNMO compared with the $LiMn_2O_4$, it is plausible that such side reactions will be more severe for LNMO/LTO full-cells. The Li^+ consumption mechanism via electrolyte decomposition on LTO needs to be determined in future studies.

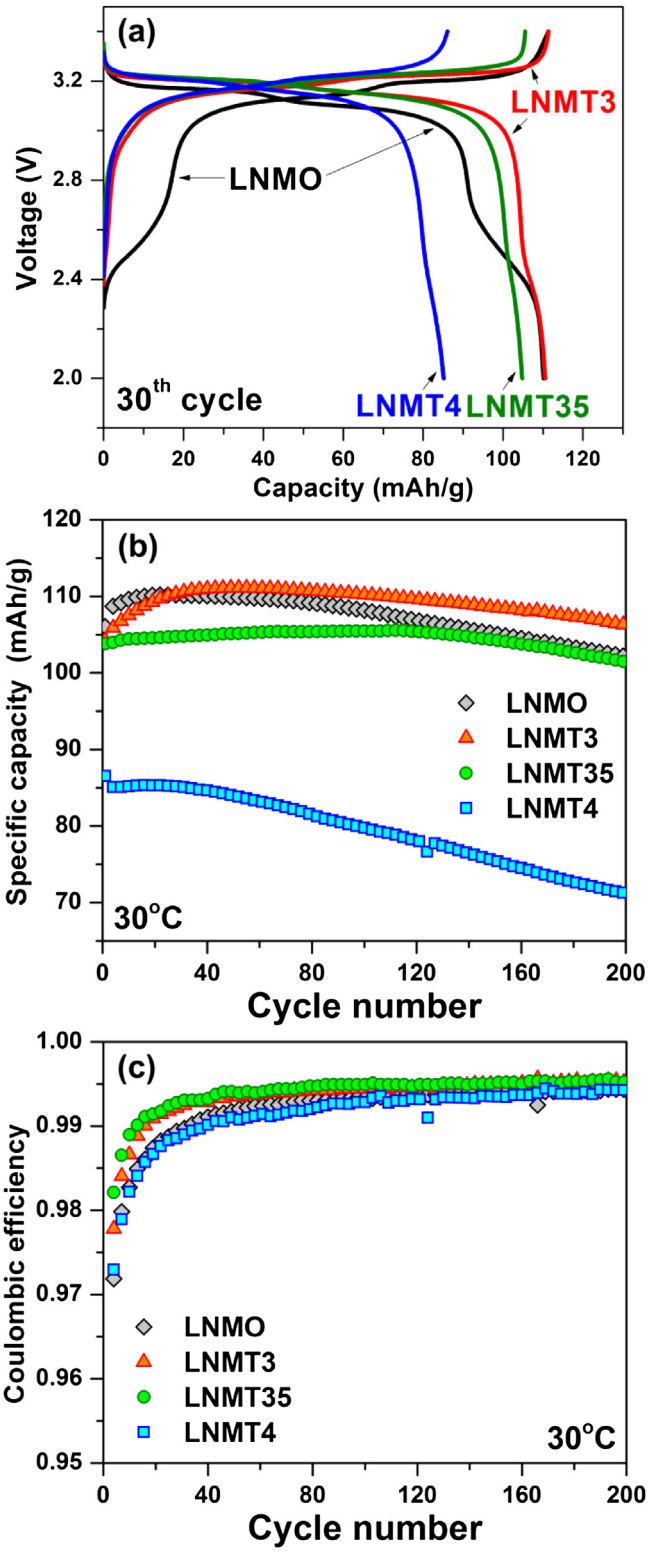

Fig. 10. (a) Representative voltage profiles of $LiNi_{0.5}Mn_{1.5-x}Ti_xO_4$ ($x = 0$, 0.3, 0.35, and 0.4)/LTO full-cells at the 30th cycle at 30 °C. (b) Cycling performances and (c) Coulombic efficiencies of the full-cells with C/5-rate at 30 °C.

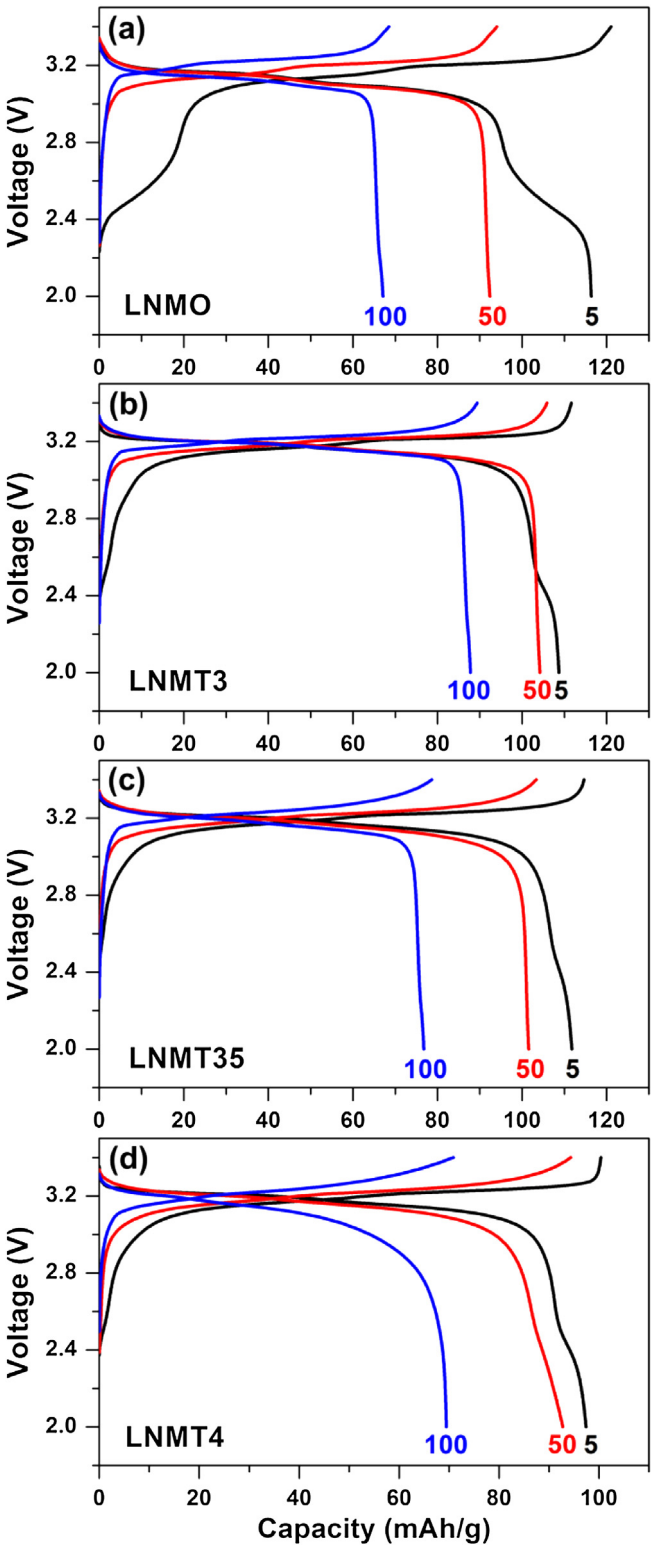

Fig. 11. Variation of voltage profiles in $LiNi_{0.5}Mn_{1.5-x}Ti_xO_4$/LTO full-cells with cycle numbers at 45 °C; (a) $x = 0$, (b) $x = 0.3$, (c) $x = 0.35$, and (d) $x = 0.4$. The full-cells were cycled in a voltage range of 2.0–3.4 V with C/5-rate.

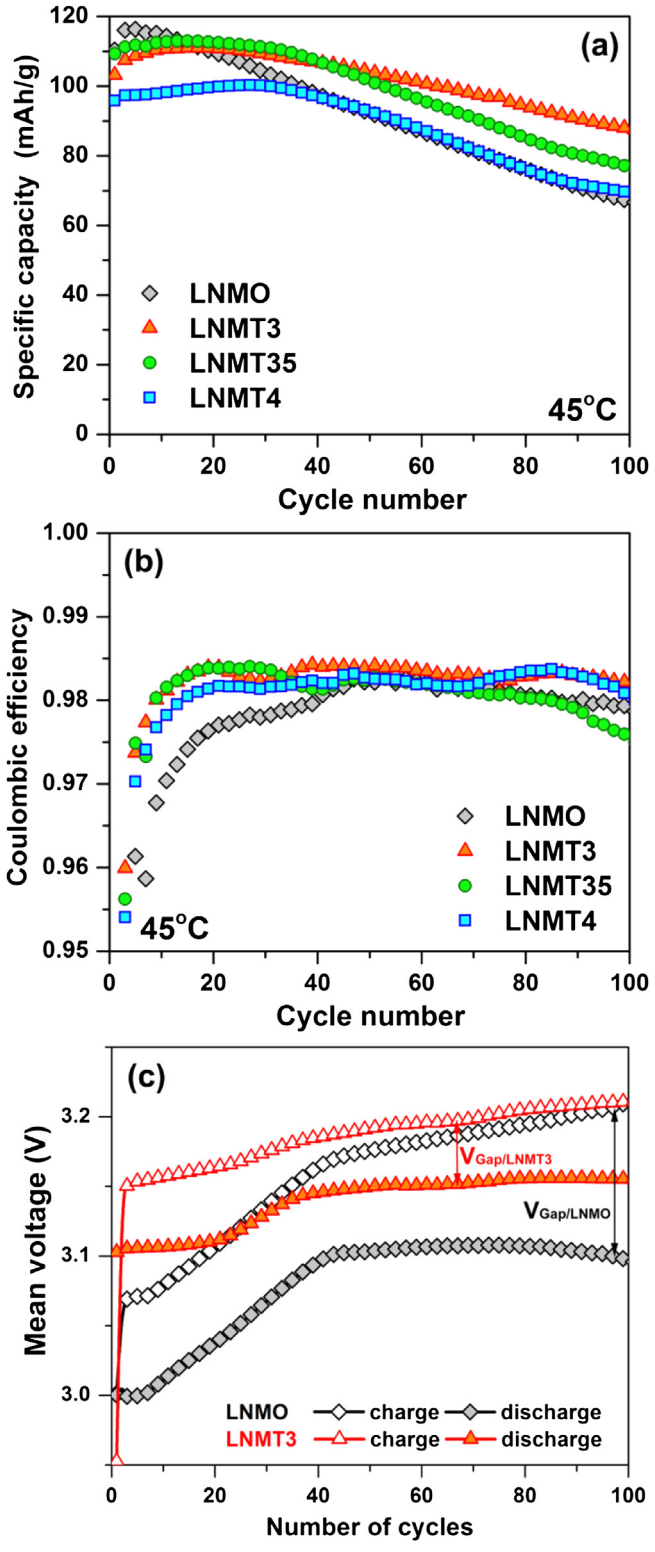

Fig. 12. (a) Variations of mean voltages on charge (open) and discharge (closed) with number of cycles, (b) cycling performances, and (c) Coulombic efficiencies of $LiNi_{0.5}Mn_{1.5-x}Ti_xO_4$/LTO full-cells with C/5-rate at 45 °C.

Fig. 13(c) and (d) demonstrates that the LNMT3 electrode suffers from Li^+ loss during cycling, like the LNMO electrode does. However, Fig. 12(c) shows that the LNMT3/LTO full-cell maintained a similar level of polarization between mean charge and discharge voltages during 100 cycles, while the polarization issue is still manifested in the LNMO/LTO full-cell. This result again supports the claim that full-cells experience less electrolyte decomposition and subsequently less parasitic reactions by employing the LNMT3 electrode.

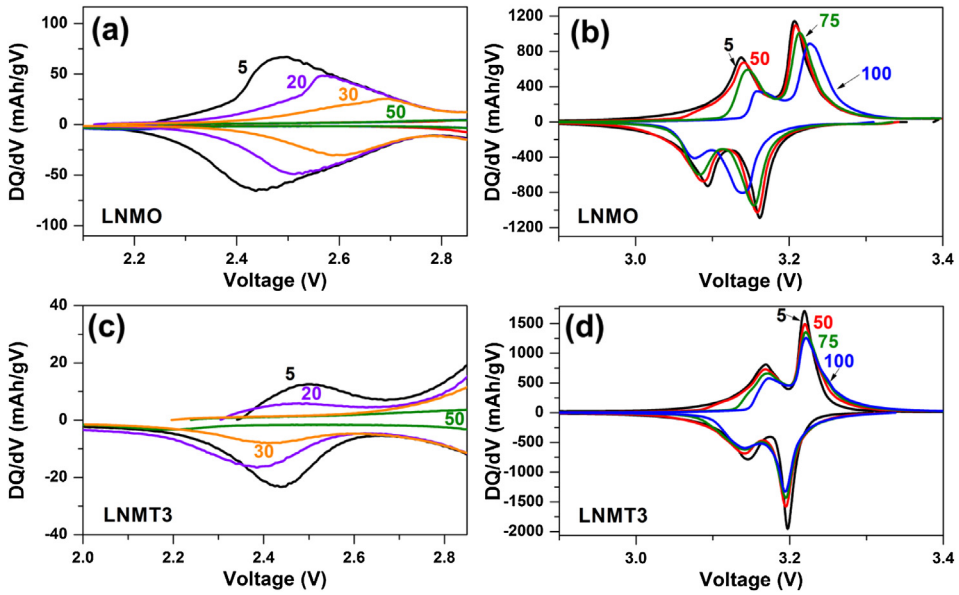

Fig. 13. Variation of *dQ*/*dV* profiles with number of cycles for (a, b) LNMO and (c, d) LNMT3 positive electrodes in $LiNi_{0.5}Mn_{1.5-x}Ti_xO_4$ ($x = 0$ and 0.3)/LTO full-cells at 45 °C.

Although the electrolyte oxidation problem still presents, employing LTO as the negative electrode in full-cells will mitigate the reductive decomposition of the electrolyte. For this reason, unlike the case of $LiNi_{0.5}Mn_{1.5-x}Ti_xO_4$/graphite full-cells, the EC/DEC (1/2 vol. ratio) based electrolyte delivered similar cycle lives to the EC/EMC (1/1 vol. ratio) based electrolyte in the $LiNi_{0.5}Mn_{1.5-x}Ti_xO_4$/LTO full-cells at 45 °C; it should be remembered that the $LiNi_{0.5}Mn_{1.5-x}Ti_xO_4$/graphite full-cells were not cycleable at 45 °C using the EC/DEC (1/2 vol. ratio) based electrolyte, as mentioned earlier. By suppressing the oxidative electrolyte decomposition, the Ti-substituted $LiNi_{0.5}Mn_{1.5-x}Ti_xO_4$ electrodes showed improved capacity retentions and Coulombic efficiencies compared with those of the LNMO. For example, Fig. 12 shows that the LNMT3 electrode delivers higher capacity retention (79%) and Coulombic efficiency (98.4%) than those of LNMO. Especially, the Ti-substituted $LiNi_{0.5}Mn_{1.5-x}Ti_xO_4$ electrodes showed good capacity retentions during initial 30 cycles, while they started to show capacity fading afterward, probably because of electrolyte degradations.

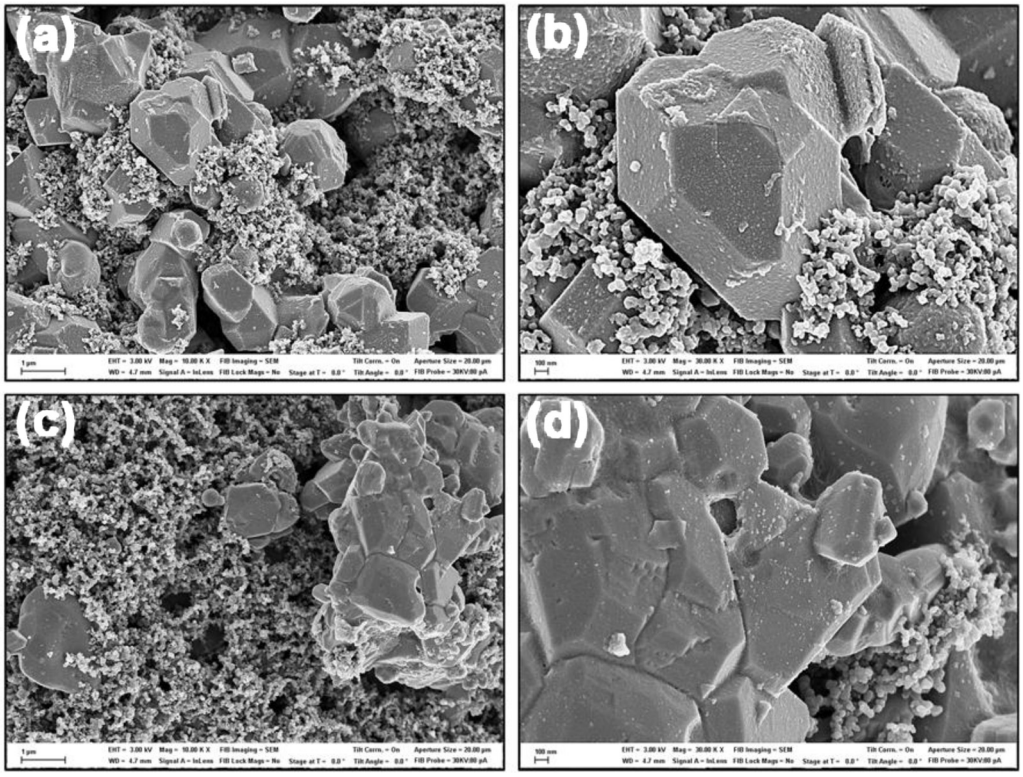

Fig. 14. SEM images of cycled positive electrodes at 30 °C: (a, b) cycled LNMO electrode and (c, d) cycled LNMT3 electrode.

Fig. 14 compares SEM images of cycled $LiNi_{0.5}Mn_{1.5-x}Ti_xO_4$ ($x = 0$ and 0.3) electrodes recovered from $LiNi_{0.5}Mn_{1.5-x}Ti_xO_4$/graphite full-cells after cycling at 30 °C. In Fig. 14(a) and (b), surfaces of LNMO electrode showed textures, which can be attributed to either transition metal dissolution or the deposition of products of electrolyte decomposition [7,28–30]. The deposits on the LNMO particles could be polymeric species and/or inorganic fluoride and phosphate species [7,31,32]. For instance, there are several literature reports of the deposition of MnF_2 on the surface of LNMO particles [7,30]. In comparison, SEM images of the cycled LNMT3 electrode appear to be relatively clean after cycling, as shown in Fig. 14(c) and (d). This result again supports that electrolyte decomposition and resulting parasitic reactions are mitigated by employing the Ti-substituted LNMT3 electrode.

Our results demonstrated that the Ti-substituted $LiNi_{0.5}Mn_{1.5-x}Ti_xO_4$ electrodes delivered improved full-cell performances paired with graphite and LTO negative electrodes in terms of cell operation voltage, polarization, cycle life, and Coulombic efficiency. It is believed that the electrolyte oxidation is mitigated by employing LNMT3 and LNMT35 electrodes, as evidenced by low self-discharge capacities (see, Fig. 5) and high Coulombic efficiencies. Among the various samples investigated, the LNMT3 delivered optimal battery performances in both graphite and LTO full-cells. Considering the similar surface areas between LNMO (1.154 $m^2\ g^{-1}$) and LNMT3 (1.112 $m^2\ g^{-1}$) powders, the difference in surface area cannot explain the improved performance of LNMT3. Future studies will focus on revealing the improvement mechanism of $LiNi_{0.5}Mn_{1.5-x}Ti_xO_4$ full-cells.

4. Conclusions

In this work, we systematically investigated the effects of Ti substitution for Mn on the electrochemical performance of $LiNi_{0.5}Mn_{1.5-x}Ti_xO_4$ (LNMTO) spinel.

1. Without Ti substitution, LNMO delivers poor capacity retention in full-cells paired with the graphite and $Li_4Ti_5O_{12}$ (LTO) negative electrodes. The capacity loss is primarily attributed to electrolyte oxidation.
2. Ti substitution in LNMO retards electrolyte oxidation, as evidenced by low self-discharge and high Coulombic efficiency. As a result, LNMTO ($x = 0.3–0.4$)/graphite full-cells delivered improved capacity retention (87–89% after 100 cycles) compared with that of the LNMO/graphite (72% after 100 cycles) at 30 °C.
3. The cleanliness of the cycled LNMTO particles observed in SEM images suggests the negligible amount of electrolyte oxidation reaction products, and provides further support for the hypothesis that Ti substitution retards electrolyte oxidation.
4. When LNMTO is paired with LTO negative electrode, electrolyte reduction is also reduced because of the high operation voltage of LTO (ca. 1.5 V vs. Li). LNMTO/LTO full-coin cells showed greater capacity retention than LNMTO/graphite.
5. At elevated temperature (45 °C), Ti-substituted LNMTO ($x = 0.3$) delivered improved capacity retention (79% after 100 cycles) as compared with Ti-free LNMO/LTO full-cells (58% after 100 cycles).

The improvement mechanism(s) of the LNMTO full-cells paired with graphite and LTO negative electrodes needs to be investigated further.

Acknowledgments

The authors would like to thank Michael P. Balogh and Anne Dailly in the Chemical & Materials Systems Laboratory for SEM and BET analyses, respectively.

References

[1] J.-H. Kim, S.-T. Myung, C.S. Yoon, S.G. Kang, Y.-K. Sun, Chem. Mater. 16 (2004) 906.
[2] J.-H. Kim, S.-T. Myung, Y.-K. Sun, Electrochim. Acta 49 (2004) 219.
[3] K. Ariyoshi, Y. Iwakoshi, N. Nakayama, T. Ohzuku, J. Electrochem. Soc. 151 (2004) A296.
[4] J.B. Goodenough, Y. Kim, Chem. Mater. 22 (2010) 587.
[5] D. Aurbach, B. Markovsky, Y. Talyossef, G. Salitra, H.-J. Kim, S. Choi, J. Power Sources 162 (2006) 780.
[6] J.-H. Kim, N.P.W. Pieczonka, Z. Li, Y. Wu, S. Harris, B.R. Powell, Electrochim. Acta 90 (2013) 556.
[7] N.P. Pieczonka, Z. Liu, P. Lu, K.L. Olson, J. Moote, B.R. Powell, J.-H. Kim, J. Phys. Chem. C 117 (2013) 15947.
[8] N.M. Asl, J.-H. Kim, N.P.W. Pieczonka, Z. Liu, Y. Kim, Electrochem. Commun. 32 (2013) 1.
[9] K.W. Leitner, H. Wolf, A. Garsuch, F. Chesneau, M. Schulz-Dobrick, J. Power Sources 244 (2013) 548.
[10] J.-H. Kim, S.-T. Myung, C.S. Yoon, I.-H. Oh, Y.-K. Sun, J. Electrochem. Soc. 151 (2004) A1911.
[11] T. Noguchi, I. Yamazaki, T. Numata, K. Utsugi, in: The Electrochemical. Society Meeting Abstracts, 2011, 1378.
[12] N. Amdouni, K. Zaghib, F. Gendron, A. Mauger, C.M. Julien, Ionics 12 (2006) 117.
[13] S. Ivanova, E. Zhecheva, R. Stoyanova, D. Nihtianova, S. Wegner, P. Tzvetkova, S. Simova, J. Phys. Chem. C 115 (2011) 25170.
[14] J.-H. Kim, A. Huq, M. Chi, N.P.W. Pieczonka, E. Lee, M. Tessema, C.A. Bridges, A. Manthiram, K.A. Persson, Submitted for publication.
[15] H. Kawai, M. Tabuchi, M. Nagata, H. Tukamoto, A.R. West, J. Mater. Chem. 8 (1998) 1273.
[16] S. Patoux, L. Daniel, C. Bourbon, H. Lignier, C. Pagano, F. Le Cras, S. Jouanneau, S. Martinet, J. Power Sources 189 (2009) 344.
[17] R. Baddour-Hadjean, Y. Dridi, J.-P. Pereira-Ramos, in: The Electrochemical. Society Meeting Abstracts, 2013, 949.
[18] P. Arora, R.E. White, M. Doyle, J. Electrochem. Soc. 145 (1998) 3647.
[19] J. Christensen, J. Newman, J. Electrochem. Soc. 152 (2005) A818.
[20] K. Nakura, Y. Ohsugi, M. Imazaki, K. Ariyoshi, T. Ohzuku, J. Electrochem. Soc. 158 (2011) A1243.
[21] J.-H. Kim, N.P.W. Pieczonka, L. Yang, ChemPhysChem (2014) in press.
[22] S.E. Sloop, J.B. Kerr, K. Kinoshita, J. Power Sources 119–121 (2003) 330.
[23] D.H. Jang, S.M. Oh, J. Electrochem. Soc. 144 (1997) 3342.
[24] T. Kawamura, S. Okada, J. Yamaki, J. Power Sources 156 (2006) 547.
[25] M. Wohlfahrt-Mehrens, C. Vogler, J. Garche, J. Power Sources 127 (2004) 58.
[26] J. Vetter, P. Novák, M.R. Wagner, C. Veit, K.-C. Möller, J.O. Besenhard, M. Winter, M. Wohlfahrt-Mehrens, C. Vogler, A. Hammouche, J. Power Sources 147 (2005) 269.
[27] B. Ravdel, K. Abraham, R. Gitzendanner, J. DiCarlo, B. Lucht, C. Campion, J. Power Sources 119–121 (2003) 805.
[28] I. Belharouak, G.M. Koenig, T. Tan, H. Yumoto, N. Ota, K. Amine, J. Electrochem. Soc. 159 (2012) A1165.
[29] N.P.W. Pieczonka, L. Yang, M.P. Balogh, B.R. Powell, K. Chemelewski, A. Manthiram, S.A. Krachkovskiy, G.R. Goward, M. Liu, J.-H. Kim, J. Phys. Chem. C 117 (2013) 22603.
[30] D. Kim, S. Park, O.B. Chae, J.H. Ryu, Y.-U. Kim, R.-Z. Yin, S.M. Oh, J. Electrochem. Soc. 159 (2012) A193.
[31] X. Fang, N. Ding, X.Y. Feng, Y. Lu, C.H. Chen, Electrochim. Acta 54 (2009) 7471.
[32] Y. Talyosef, B. Markovsky, G. Salitra, D. Aurbach, H.-J. Kim, S. Choi, J. Power Sources 146 (2005) 664.